

UNIVERSITY OF OKLAHOMA
GRADUATE COLLEGE

**Scalable Multipartite Entanglement Using
Squeezed Light**

A THESIS
SUBMITTED TO THE GRADUATE FACULTY
in partial fulfillment of the requirements for the
Degree of
MASTER OF SCIENCE

By

DAIDA THOMAS
Norman, Oklahoma
2022

Scalable Multipartite Entanglement Using Squeezed Light

A THESIS APPROVED FOR THE
HOMER L. DODGE DEPARTMENT OF PHYSICS AND ASTRONOMY

BY THE COMMITTEE CONSISTING OF

Dr. Alberto Marino Valle, Chair

Dr. Eric Abraham

Dr. Arne Schwettmann

Dr. Bruno Barboza

Dr. Binbin Weng

Copyright by DAIDA THOMAS 2022
All Rights Reserved.

To Light

Not the laser light using which I conducted all the work reported here. But to the light of the world. To Him, through whom I live, move and have my being.

"In him was life and that life was the light of all mankind. The light shines in the darkness, and the darkness has not overcome it" [John 1:4].

Acknowledgments

To Dr. Alberto M. Marino for taking me in as I am, and moulding me into a good experimentalist. His patience, guidance and motivation has enabled me to grow, to learn and to make a better physicist out of myself. To my committee members for their continued guidance and support.

I am grateful to Saesun for making me a part of this project. Working alongside a long way, he was patient and understanding with me and always made himself available in times of requirement. I would also like to thank my academic brothers Javad, Tim, Umang and Kit for their constant support, suggestions and help while conducting this work.

Gaurav, you taught me the first lesson of research, that we are people who get paid for doing what we love. You taught me that experimentalists face problems and their life is about looking for solutions. The time you have taken to explain things and for making me comfortable in the lab will forever be a lesson on how to treat others and my work, unselfishly and with full dedication.

To my dear friend Veena Balakrishnan for her constant encouragement and love throughout my time in Norman. To Geo, for spending a short time with me, for his listening heart and thoughtful words.

Words cannot express my heart of gratitude to my beloved parents, Thomas and Vijayalakshmi, to my sisters Cigole and Loria, and to my friends Jyothi and Veena P.R. for loving me unconditionally in the darkest of nights and brightest of days. Their love, companionship and prayers held me together and have been a constant source of energy booster in my life.

To my dearest friends Camryn and Emily, for their fellowship and for encouraging me to abide in the love of Christ. To Sooners for Christ members, Alameda church family and to my parents Lois and Henry, Julie and Lynn, for their heart to serve and love GOD.

To Shawn, for the beautiful memories you left behind. For smiling and crying with me, for being a wonderful friend and for loving me as I am while being with me.

Above all, I want to thank GOD whom I fearlessly call *Abba* and my Lord JESUS CHRIST for teaching, reproof, training and for correcting me in righteousness. Your disciplining in love enabled me to identify the problems and look for solution which I found and embraced in the truth and reality. You taught me to believe when I couldn't even look upon myself. Your love will be my portion and shield forever. As Lord declared to Abraham in Genesis 15:1, my heart recites,

"I won't be afraid. The LORD is my shield and my very great reward".

Abstract

Quantum entanglement is a pure quantum mechanical phenomena with no classical counterpart. The strong non locality of multipartite entangled states makes it suitable for application of quantum mechanics towards quantum computing, quantum key distribution and quantum interferometry. Many methods have been proposed for the generation of scalable multipartite entangled states in the frequency domain and by time-bin multiplexing. However, these are not suitable for long distance quantum communication. To build a long distance quantum network, we need a spatially separable multipartite entangled system. In this thesis, we focus on the use of a quantum interferometer, known as the $SU(1,1)$ interferometer formed using a two mode squeezed quantum state, to generate a multipartite entangled quantum system in the spatial domain.

We start with an introduction to the basic properties of quantum states of light and entangled systems. Later, we expand on the scheme proposed for the generation of multipartite entangled system. We go over the experimental implementation of this scheme and experimentally verify the existence of multipartite quantum correlated state.

Contents

Dedication	iv
Acknowledgments	v
Abstract	vi
1 Introduction	1
2 States of the Electromagnetic Field	3
2.1 Uncertainties in field quadratures	3
2.2 Coherent states	4
2.3 Single mode squeezed state	6
2.4 Two mode squeezed state	6
3 Quantum Entanglement	8
3.1 Entangled states	8
3.2 Multimode squeezing and entanglement	10
3.3 Generation of squeezed light	12
3.3.1 Four wave mixing	13
3.3.2 Multi-spatial mode nature of twin beams	13
3.4 Generation of scalable multipartite entanglement	15
4 Experimental Implementation and Results	17
4.1 Measurements of intensity-intensity correlations	18
4.2 Measurements of noise between uncorrelated modes	19
5 Conclusion and future work	22

Chapter 1

Introduction

Quantum states of light, such as squeezed and entangled states, that contain correlations beyond the classical limit are attractive on several fronts. For example, the reduced noise properties of squeezed states allow high precision measurements^[1], enhanced resolution for quantum imaging applications^[2,3], and enhanced sensitivity of measurements with optical devices^[4,5]. On the other hand, the strong nonlocality of entangled states makes them a key ingredient in quantum information science^[6].

A composite quantum system consisting of more than two entangled subsystems is called a multipartite entangled state. These states carry shared information and hence its advantageous for applications such as secure quantum communication and quantum computing^[6]. Different techniques for the generation of multipartite entangled states have been theoretically proposed and experimentally implemented both in the discrete variable (DV) regime by exploiting the properties of individual photons and in the continuous variable (CV) regime that treats optical field as waves. In contrast to the DV regime where the measurements are probabilistic, in CV regime operations can be deterministically performed for quadrature variables of the electromagnetic field. Squeezed light is a valuable ingredient for CV entanglement as we can generate quantum correlations between the quadratures of different modes through the process of squeezing.

A standard technique for the generation of CV multipartite entanglement (CVME) is based on mixing squeezed states on linear beam splitters^[7,8] or using cascaded amplifier networks^[9]. However, these techniques are not easily scalable, as the correlations can degrade due to mode mismatch or optical losses. To overcome these limitations, one or two quantum states composed of multiple modes can be used. This approach has been experimentally implemented with temporal modes from a parametric oscillator^[10]. Entangled multimodes have also been generated for different spatial regions in a single beam^[11]. Additionally, a scalable technique for the generation of genuine CVME has been demonstrated through the use of time bin multiplexing of squeezed light sources in the temporal domain^[12].

Prior work from our group proposed a theoretical scheme for the generation of genuine scalable CVME based on spatial modes^[13]. This proposal consists of a $SU(1,1)$ -like interferometer with two four wave mixing (FWM) processes serving as the source and mixing elements for the multiple spatial modes contained in two optical beams. The setup contains only two active elements and provides a more straightforward and scalable technique

for the generation and verification of genuine multipartite entanglement in the spatial domain. In this report, we present our preliminary experimental results on the implementation of this technique.

Chapter 2

States of the Electromagnetic Field

In the CV regime, the measurable quantities associated with an optical field are the quadratures of the electric field. To better understand their quantum properties, we first introduce the uncertainties and noise properties satisfied by these quadratures. We then present the properties of different states, such as coherent states and squeezed states of light.

2.1 Uncertainties in field quadratures

By expanding the vector potential of the EM field in terms of cavity modes we can quantize the field using harmonic oscillators corresponding to every individual cavity mode. An EM field with angular frequency ω confined in a cavity of volume V , can be expressed in the quantized form as^[14]

$$\hat{E}(z, t) = E_0(\hat{a}e^{-i\omega t} + \hat{a}^\dagger e^{i\omega t}). \quad (2.1)$$

Here $E_0 = \sqrt{\frac{\hbar\omega}{V}}$, and \hat{a} and \hat{a}^\dagger are the annihilation and creation operators of the number of photons in the field. Since photons are bosons, they obey the bosonic commutation relation $[\hat{a}, \hat{a}^\dagger] = 1$. This expression can be conveniently rewritten as

$$\hat{E}(z, t) = \epsilon(\hat{X} \cos \omega t + \hat{Y} \sin \omega t). \quad (2.2)$$

where the real and imaginary parts \hat{X} and \hat{Y} respectively are also called the quadratures of the field. These quadratures are the experimentally measurable quantities of the field. The field quadratures in terms of the bosonic field operators are given by $\hat{X} = \frac{1}{2}(\hat{a} + \hat{a}^\dagger)$ and $\hat{Y} = \frac{1}{2i}(\hat{a} - \hat{a}^\dagger)$ ^[15]. They satisfy the commutation relation $[\hat{X}, \hat{Y}] = \frac{i}{2}$ and it can be shown that they obey the uncertainty relation,

$$\langle \Delta \hat{X}^2 \rangle \langle \Delta \hat{Y}^2 \rangle \geq \frac{1}{16}. \quad (2.3)$$

The variance of the operators gives a measure of the noise associated with the measurement of observables \hat{X} and \hat{Y} for that quantum state and this uncertainty limits the noise associated with the corresponding state. A state containing no photons, called the vacuum state, minimizes the uncertainty product in Eq. 2.3 with equal noise in both quadratures .i.e.,

$$\langle \Delta \hat{X}^2 \rangle = \frac{1}{4} = \langle \Delta \hat{Y}^2 \rangle. \quad (2.4)$$

The noise level of this state with equal fluctuations in both quadratures is called the standard quantum limit (SNL). The SNL is the minimum noise limit achievable with a classical state of light. Quantum correlations can lead to uncertainties beyond their corresponding classical counterpart in one quadrature at the expense of increased noise in the other quadrature.

2.2 Coherent states

An appropriate basis state to represent an optical field involving large number of photons is a coherent state, denoted by $|\alpha\rangle$. This state minimizes the uncertainty relation given in Eq. 2.3 with equal uncertainties in each of the quadratures. That is, for a coherent state, the quadrature variances are $\langle \Delta \hat{X}^2 \rangle = \langle \Delta \hat{Y}^2 \rangle = \frac{1}{4}$. This shows that coherent states have quadrature fluctuations equal to those of a vacuum state.

A classical phase space diagram gives us the trajectory of a particle with respect to its position and momentum. Similarly, we can visualize the field using a phase space diagram where the trajectory is drawn with respect to the in phase, \hat{X} , and out of phase, \hat{Y} , components of the field. The equality in quadrature variances will lead to an isotropic phase space diagram for a coherent state as shown in Fig. 2.1a. The x axis and y axis represent the amplitude and phase quadratures respectively. The distance from the origin gives the amplitude and phase of the field and the distribution of circle gives the noise arising due to uncertainty. Unlike in classical mechanics, the state at a particular time is not confined to a single point due to the uncertainty in measurements of the field quadratures.

Coherent states can be generated by displacing a vacuum state using the unitary displacement operator, $\hat{D}(\alpha)$, such that

$$|\alpha\rangle = \hat{D}(\alpha) |0\rangle \quad (2.5)$$

with complex amplitude $\alpha = |\alpha|e^{i\phi}$ and $\hat{D}(\alpha)$ given by

$$\hat{D}(\alpha) = e^{(\alpha\hat{a}^\dagger - \alpha^*\hat{a})} [15]. \quad (2.6)$$

In phase space, a vacuum state can be represented by a circle centered at the origin, whereas the coherent state is displaced from the origin by a magnitude $|\alpha|$ and an angle ϕ . In Fig. 2.1a, a state with $\phi = 0$ is shown. The real part of α will give us the expectation value of the \hat{X} quadrature, whereas the imaginary part of α gives the mean value of the \hat{Y} quadrature.

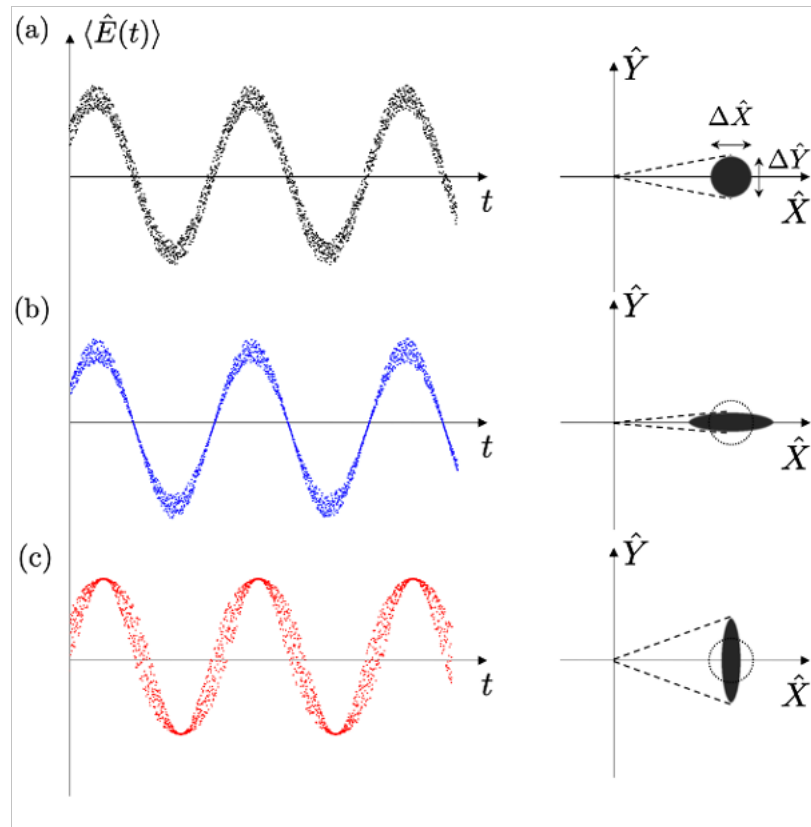


Figure 2.1: Electric field as a function of time and the corresponding phase space diagram showing the uncertainty in the phase and amplitude quadratures for a) a coherent state b) a phase squeezed state c) an amplitude squeezed state (Adapted from^[16]).

2.3 Single mode squeezed state

It is possible to reduce the noise in one quadrature below that of a coherent state at the expense of increased noise in the other quadrature so as to still satisfy the uncertainty relation in Eq. 2.3. A squeezed state is such a state. As shown in Fig. 2.1b if the noise in the phase quadrature is reduced at the expense of increased noise in the amplitude quadrature the state is called a phase squeezed state. On the other hand, if the fluctuations in the amplitude are decreased with increased fluctuations in the phase, the state is called an amplitude squeezed state, Fig. 2.1c.

The unitary operator to generate a single mode squeezed state, $\hat{S}(\epsilon)$ is defined as^[15]

$$\hat{S}(\epsilon) = \exp\left(\frac{1}{2}\epsilon^* \hat{a}^2 - \frac{1}{2}\epsilon \hat{a}^{\dagger 2}\right) \quad (2.7)$$

where $\epsilon = r e^{i\theta}$ is the squeezing parameter, r is the degree of squeezing, and θ is the squeezing phase. The amount of squeezing depends on the value of r . From the expression for the squeezing operator, it is evident that squeezing requires the production or annihilation of photons in pairs. If \hat{X} is the squeezed and \hat{Y} is the antisqueezed quadrature, then

$$\langle \Delta \hat{X}^2 \rangle < \frac{1}{4} \quad \text{and} \quad \langle \Delta \hat{Y}^2 \rangle > \frac{1}{4}.$$

Apart from this, if the product of uncertainties satisfy the equality sign in Eq. 2.3, it is a minimum uncertainty state and is called an ideal squeezed state. For a squeezed state, the compression and elongation along two axes lead to an uncertainty ellipse in the phase space as shown in Figs. 2.1b and 2.1c.

2.4 Two mode squeezed state

Instead of squeezing a single mode of the electromagnetic field, two or more modes of the field can exhibit squeezing in joint quadratures. The simplest example is the two mode squeezed state. Analogous to the single mode squeezing operator, we can define a two mode squeezing operator, which acts on both modes of the state according to^[15]

$$\hat{S}_{ab}(\epsilon) = \exp\left(\epsilon^* \hat{a} \hat{b} - \epsilon \hat{a}^\dagger \hat{b}^\dagger\right) \quad (2.8)$$

with the operators, \hat{a} and \hat{b} , being the annihilation operators of two different modes. In this process, two photons are emitted simultaneously into two different modes of the field. These operators satisfy the commutators $[\hat{a}, \hat{a}^\dagger] = 1$, $[\hat{b}, \hat{b}^\dagger] = 1$, $[\hat{a}, \hat{b}] = 0$, $[\hat{a}^\dagger, \hat{b}^\dagger] = 0$, $[\hat{a}, \hat{b}^\dagger] = 0$, $[\hat{a}^\dagger, \hat{b}] = 0$. In contrast to single mode squeezing, here squeezing does not exist in individual modes, but in the correlated states described by the combination of modes (two in this case)^[14]. If we measure the noise in the individual quadratures of each mode, it will go above the SNL level, that is

$$\langle \Delta \hat{X}_a^2 \rangle > \frac{1}{4}, \quad \langle \Delta \hat{X}_b^2 \rangle > \frac{1}{4} \quad \text{and} \quad \langle \Delta \hat{Y}_a^2 \rangle > \frac{1}{4}, \quad \langle \Delta \hat{Y}_b^2 \rangle > \frac{1}{4}, \quad (2.9)$$

so that each mode by itself is not squeezed. Here \hat{X}_a, \hat{Y}_a and \hat{X}_b, \hat{Y}_b corresponds to the quadratures of modes \hat{a} and \hat{b} , respectively.

Additionally, the two mode squeezing operator $\hat{S}_{ab}(\epsilon)$, given in Eq. 2.8, cannot be written as the product of two single mode squeezing operators $\hat{S}_a(\epsilon)$ and $\hat{S}_b(\epsilon)$ of the individual modes. However, we can rewrite $\hat{S}_{ab}(\epsilon)$ as a factorized product of two single mode squeezing operators of new modes, such that^[17]

$$\exp(\epsilon \hat{a}^\dagger \hat{b}^\dagger - \epsilon^* \hat{a} \hat{b}) = \exp\left(\frac{\epsilon}{2} \hat{d}^{\dagger 2} - \frac{\epsilon^*}{2} \hat{d}^2\right) \exp\left(\frac{-\epsilon}{2} \hat{c}^{\dagger 2} + \frac{\epsilon^*}{2} \hat{c}^2\right). \quad (2.10)$$

Here \hat{c} and \hat{d} are commuting operators that are linear combinations of \hat{a} and \hat{b} , such that $\hat{c} = \frac{\hat{a}-\hat{b}}{\sqrt{2}}$ and $\hat{d} = \frac{\hat{a}+\hat{b}}{\sqrt{2}}$ with $[\hat{c}, \hat{c}^\dagger] = 1$, $[\hat{d}, \hat{d}^\dagger] = 1$, $[\hat{c}, \hat{d}] = 0$, $[\hat{c}^\dagger, \hat{d}^\dagger] = 0$, $[\hat{c}, \hat{d}^\dagger] = 0$, $[\hat{c}^\dagger, \hat{d}] = 0$. From Eq. 2.10 it is evident that in two mode squeezed state, squeezing exists between different combinations of quadratures. Therefore, in order to observe squeezing we need to define the combined quadratures

$$\hat{X} = \frac{\hat{X}_a - \hat{X}_b}{\sqrt{2}}, \quad \hat{Y} = \frac{\hat{Y}_a + \hat{Y}_b}{\sqrt{2}}. \quad (2.11)$$

Since the commutator of these joint \hat{X} and \hat{Y} quadratures vanishes, they are simultaneously measurable and will both be squeezed. For displacement of the two modes in phase space along x axis and $\theta = 0$, the reduced noise in the joint quadrature is given by,

$$\langle \Delta \hat{X}^2 \rangle = \exp(-2r) \quad \text{and} \quad \langle \Delta \hat{Y}^2 \rangle = \exp(-2r).$$

Chapter 3

Quantum Entanglement

The properties of a quantum system depend on the interaction through which it is generated. Such interactions can lead to an interesting quantum mechanical phenomenon called entanglement. Sometimes, when two or more physical systems interact with each other certain nonclassical correlations emerge between the systems, that can persist even if the systems are separated in space (spatial separation) or time (temporal separation). In other words entanglement describes an ensemble of systems that are not independent with respect to one or more of its properties, such as position, momentum, or spin.

Now, the next fundamental question to ask is which states are entangled and which ones are not. There are certain criteria that are necessary and sufficient to prove the presence of entanglement. In this chapter, we look at the definition of entanglement and identify multimode squeezed state as a source of entanglement. Along with that we will briefly discuss some criteria to be tested for the existence of entanglement in two or more squeezed modes, followed by the method adopted for the generation of scalable multipartite entanglement.

3.1 Entangled states

Consider two subsystems \mathcal{A} and \mathcal{B} with associated Hilbert state spaces $\mathcal{H}_{\mathcal{A}}$ and $\mathcal{H}_{\mathcal{B}}$. The composite system $\mathcal{A}+\mathcal{B}$ is associated with the tensor product space $\mathcal{H}_{\mathcal{A}} \otimes \mathcal{H}_{\mathcal{B}}$. Some state vectors of the composite system can be decomposed into a tensor product of two vectors, one describing the state of the subsystem \mathcal{A} and other describing the state of the subsystem \mathcal{B} , e.g.,

$$|\Psi\rangle = |A\rangle \otimes |B\rangle. \quad (3.1)$$

Such a state is called a separable state and here, the subsystems are independent of each other. However, if the two subsystems were not prepared independently and in total isolation from each other, a decomposition of $|\Psi\rangle$ in the form given in Eq. 3.1 is not always possible and the state is called an inseparable or entangled state. The most famous example of such a bipartite entangled state is the state of two spin 1/2 particles with the total spin

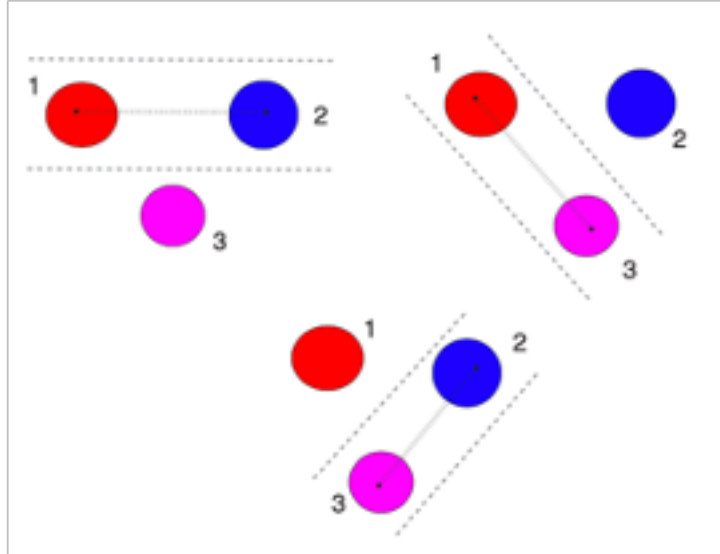


Figure 3.1: Possible bipartitions in a tripartite system. The inseparability in each case confirms the full inseparability of the composite system. (Adapted from^[18]).

angular momentum zero,

$$|\Psi\rangle = \frac{1}{\sqrt{2}}[|\uparrow\rangle \otimes |\downarrow\rangle + |\downarrow\rangle \otimes |\uparrow\rangle].$$

The kets $|\uparrow\rangle$ and $|\downarrow\rangle$ represent the spin up and spin down states, respectively, along the arbitrary direction.

Multipartite Entanglement

If a composite system involves more than two subsystems that are entangled, it is called a multipartite entangled (ME) system. The quantum state of one of the subsystems of an entangled pair has to be described by a density operator, which is linear in \mathcal{H} . This density operator can be associated with any subsystem, regardless of the existence of a state vector associated with that subsystem. By generalizing Eq. 3.1 in terms of the density matrix, $\rho = \sum_n p_n |\Psi_n\rangle\langle\Psi_n|$ a composite system consisting of n subsystems is fully separable if we can write the total density operator as

$$\hat{\rho} = \sum_n p_n \hat{\rho}_{n1} \otimes \hat{\rho}_{n2} \otimes \hat{\rho}_{n3} \dots \otimes \hat{\rho}_{nm}.$$

Here, $p_n \geq 0$ is the probability for the system to be in the state of $|\Psi_n\rangle$ and $\sum_n p_n = 1$. For the particular case of a state described by a state vector $|\Psi\rangle \in \mathcal{H}$, the density operator is the outer product of the state

$$\hat{\rho} = |\Psi\rangle\langle\Psi|.$$

By inspecting a system for inseparability we can verify whether it is entangled. If a ME system is inseparable with respect to all possible bipartitions, such a system is called genuine multipartite entangled (GME).

The simplest case of ME is the tripartite entangled state. In such a system, the density operator of the form

$$\hat{\rho} = \sum_n p_n \hat{\rho}_{n,12} \otimes \hat{\rho}_{n,3}$$

implies that it is in a mixture of states n . This density operator suggest that among the three parties (modes) 1, 2 and 3, the two parties 1 and 2 may be entangled or not, but 3 is not entangled with the rest. This particular bipartition is represented as (12, 3) and the permutations of 1, 2 and 3 covers all possible bipartitions. These three possible bipartitions in the case of a tripartite system are shown in Fig. 3.1. If the state of each of these bipartitions cannot be defined by a density operator of the form given above, we can confirm that it is a fully inseparable tripartite system.

3.2 Multimode squeezing and entanglement

A physically realizable and the simplest example of continuous variable bipartite entangled state is the two mode squeezed vacuum (TMSV). Here, the two subsystems \mathcal{A} and \mathcal{B} are localized modes of the electromagnetic field with corresponding bosonic operators \hat{a} and \hat{b} . These can be prepared through a nonlinear process such as four wave mixing, which is discussed in detail in the following section. The quadrature wavefunctions of the TMSV state can be written as^[6]

$$\psi(\hat{X}_1, \hat{X}_2) = \sqrt{\frac{2}{\pi}} \exp[-e^{-2r}(\hat{X}_1 + \hat{X}_2)^2/2 - e^{2r}(\hat{X}_1 - \hat{X}_2)^2/2] \quad (3.2)$$

$$\psi(\hat{Y}_1, \hat{Y}_2) = \sqrt{\frac{2}{\pi}} \exp[-e^{-2r}(\hat{Y}_1 - \hat{Y}_2)^2/2 - e^{2r}(\hat{Y}_1 + \hat{Y}_2)^2/2]. \quad (3.3)$$

They approach the limit $C\delta(X_1 - X_2)$ and $C\delta(Y_1 + Y_2)$ respectively for infinite squeezing $r \rightarrow \infty$. These states describe correlated relative \hat{X} and total \hat{Y} quadratures. This is analogous to the famous EPR entangled state treated in^[19].

In order to experimentally investigate the entanglement in this system, Duan et al.^[20] showed that the violation of an inequality involving the variances of sum and difference quadratures is sufficient to prove bipartite entanglement for a CV system. The inequality takes the form,

$$\langle [\Delta(\hat{X}_1 - \hat{X}_2)]^2 \rangle + \langle [\Delta(\hat{Y}_1 + \hat{Y}_2)]^2 \rangle \geq 2|\langle [\hat{X}, \hat{Y}] \rangle| \quad (3.4)$$

with $[\hat{X}_i, \hat{Y}_j] = \frac{i\delta_{ij}}{2}$. The LHS of Eq. 3.4 is always less than the RHS for any two mode squeezed state with a finite degree of squeezing, thereby proving that it is a bipartite entangled state. The squeezing parameter r , which determines the degree of squeezing, also determines the strength of the entanglement. In the limit of infinite squeezing, i.e., $r \rightarrow \infty$, this state will become a perfectly correlated or maximally entangled state, which is unphysical and unnormalizable. However, for a finite amount of squeezing, we will have an experimentally

achievable entangled state.

Instead of two localized modes, a large number of modes of the EM field can be jointly squeezed. For an arbitrary number of modes described by the bosonic operators,

$$\hat{a}_k = \hat{X}_k + i\hat{Y}_k$$

($k = 1, 2, \dots, N$) the correlations between the output quadratures can be verified by the reduced noise below the SNL in the relative \hat{X} ($\hat{X}_i - \hat{X}_{i+1}$) and total \hat{Y} ($\hat{Y}_i + \hat{Y}_{i+1} + \dots + \hat{Y}_N$) quadratures^[21].

$$[\hat{X}_i, \hat{Y}_j] = \frac{i\delta_{ij}}{2}$$

$$\langle [\Delta(\hat{X}_i - \hat{X}_j)]^2 \rangle = \frac{1}{4} \exp(-2r)$$

and

$$\langle [\Delta(\hat{Y}_1 + \hat{Y}_2 + \dots + \hat{Y}_N)]^2 \rangle = \frac{1}{4} \exp(-2r)$$

for $i \neq j (i, j = 1, 2, \dots, N)$

Hence for an N -partite entangled system, $N-1$ pairs of relative X and total Y quadratures will be squeezed. The sign difference in the joint quadratures of conjugate variables \hat{X} and \hat{Y} is due to the fact that the reduced noise in one quadrature implies excess noise in the other to satisfy Heisenberg's uncertainty principle. To verify multipartite entanglement in such a system, Loock and Furusawa^[22] showed that it is necessary to measure the violations of all biseparable pairs individually. These inequalities are expressed in terms of variances of squeezed quadrature combinations as

$$\langle [\Delta(\hat{X}_1 - \hat{X}_2)]^2 \rangle + \langle [\Delta(\hat{Y}_1 + \hat{Y}_2 + g_3\hat{Y}_3 + \dots + g_N\hat{Y}_N)]^2 \rangle > 1 \quad (3.5)$$

⋮

$$\langle [\Delta(\hat{X}_{N-1} - \hat{X}_N)]^2 \rangle + \langle [\Delta(g_1\hat{Y}_1 + g_2\hat{Y}_2 + g_3\hat{Y}_3 + \dots + g_{N-2}\hat{Y}_{N-2} + \hat{Y}_{N-1} + \hat{Y}_N)]^2 \rangle > 1 \quad (3.6)$$

In the above equations, \hat{X}_i' s and \hat{Y}_i' s are the two quadratures of different modes, and the g_i' s are arbitrary coefficients that can be used to minimize the sum in the \hat{Y} quadrature linear combinations. The commutator of these particular combinations of joint quadratures vanishes, thereby allowing arbitrarily good violations and the existence of simultaneous eigenstates of these combinations allows them to be simultaneously measurable. For a specific bipartition, a set of inequalities from the above equations needs to be violated to show that its density matrix cannot be decomposed. The inequalities coincide for some bipartitions and hence for the experimental verification of N -partite entanglement, only $N-1$ inequalities need to be violated given by Eq. 3.5 through Eq. 3.6.

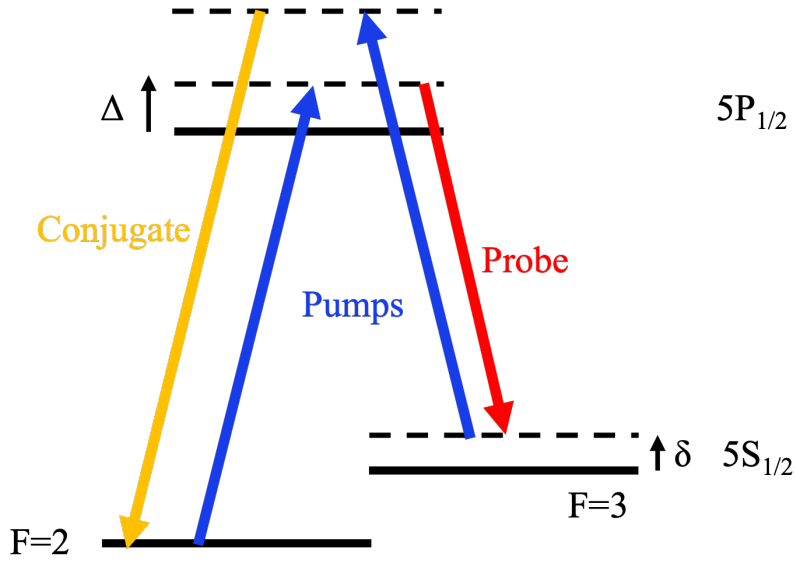


Figure 3.2: Double lambda configuration for FWM in ^{85}Rb . Two pump photons, P (purple), are absorbed to simultaneously generate a probe, pr (red), and conjugate, c (yellow), photon.

3.3 Generation of squeezed light

The response of a nonlinear medium to an external field can be written in terms of the electric dipole moment per unit volume or polarization, $\tilde{P}(t)$, as^[23]

$$\tilde{P}(t) = \epsilon_0[\chi^{(1)}\tilde{E}(t) + \chi^{(2)}\tilde{E}^2(t) + \chi^{(3)}\tilde{E}^3(t) + \dots]. \quad (3.7)$$

where χ is the susceptibility of the medium. The first term on RHS is the linear response, whereas the second, third, and other higher-order terms indicate the nonlinear response of the medium. Depending on the nonlinear coefficients of a medium and the strength of the electric field, different nonlinear effects contribute to the behavior of the medium.

The second-order nonlinear response occurs only in a medium that does not display inversion symmetry^[23]. In our experiments, we are using a nonlinear process called four wave mixing (FWM) to generate squeezed light. Due to the inversion symmetry of atoms, the $\chi^{(2)}$ term vanishes, and hence we need to use a third-order nonlinear process such as FWM that arises due to the contribution of the third term in the RHS of Eq. 3.7. The efficiency of the FWM process depends on the strength of the nonlinearity of the medium.

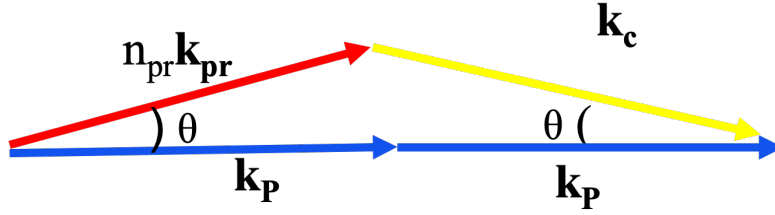


Figure 3.3: Effective phase matching condition in FWM process between pump (purple), probe (red) and conjugate (yellow) by tuning the angle θ between the beams. After the FWM process the twin beams will symmetrically move away from each other with respect to pump.

3.3.1 Four wave mixing

In the FWM process an intense light beam called the pump with frequency ω_P interacts with an atomic medium, resulting in the absorption of two pump photons and the simultaneous generation of a probe and conjugate photon. The generated beams are also called twin beams. For a single input pump beam, conservation of energy dictates that the frequencies of the annihilated and created photons satisfy

$$2\omega_P = \omega_{pr} + \omega_c, \quad (3.8)$$

where ω_P , ω_{pr} and ω_c are the frequencies of the pump, probe, and conjugate, respectively. Fig. 3.2 shows the double lambda configuration for the FWM process in the D1 line of ^{85}Rb that we use in our experiment. The difference in frequency between the pump and probe fields is equal to the two-photon detuning δ , plus the frequency difference between the ground hyperfine levels; i.e., $\omega_P - \omega_{pr} = \omega_{HF} + \delta$ where ω_{HF} is the energy difference between hyperfine levels $F=2$ and $F=3$ of the ground state $5S_{1/2}$. Efficient FWM happens when the frequency of the probe field is on resonance with the atomic transition (red) shown in Fig. 3.2. However, absorption, a linear process, suppresses the nonlinear FWM on resonance. To avoid this, we slightly detune the frequency of the pump by Δ as shown in Fig. 3.2.

It is possible to not seed the process (vacuum seed), seed with either probe or conjugate, or both beams simultaneously. If the process is not seeded, then we will have a TMSV state. However, if we seed the FWM process with an input probe, we will get a squeezed coherent state, which contains a higher number of photons. Hence, this two mode squeezed state is called a bright two mode squeezed state (bTMSS).

3.3.2 Multi-spatial mode nature of twin beams

The FWM process is a parametric process, which means that the state of the atoms before and after the process is the same. In other words, the momentum and energy are conserved by the fields. Momentum conservation

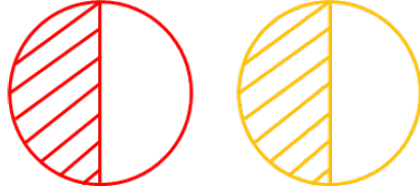


Figure 3.4: Red and yellow circle indicates probe and conjugate respectively. In the near field, corresponding regions(either shaded or unshaded) of probe and conjugate will be correlated.

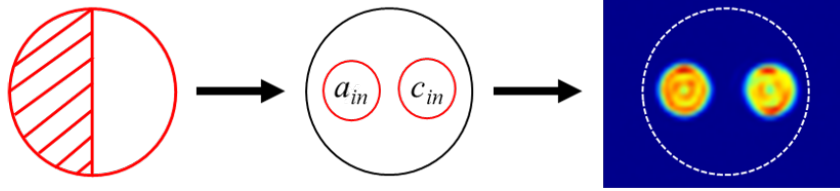


Figure 3.5: The mutli-spatial mode nature of the twin beams can be used to make spatially independent regions within the twin beams. This is acheived by encoding different patterns in the probe beam.

is more generally written in terms of wave vectors, k . For the double lambda configuration shown in Fig. 3.2, momentum conservation takes the form

$$\Delta k = 2k_P - k_{pr} - k_c. \quad (3.9)$$

Here k_P , k_{pr} and k_c are the momentum vectors of the pump, probe, and conjugate, respectively. For $\Delta k = 0$ the FWM occurs effectively. However, in general cases $\Delta k \neq 0$ and the efficiency of FWM is reduced. The phase mismatch Δk is due to the propagation angle of the twin beams and the change in the effective refractive index of the medium as seen by a beam as it propagates through the medium. This is a consequence of the dispersive behavior of the medium. Because of this, we can rewrite the phase matching condition in a more explicit form. Taking into account these factors, when the two photons from the pump are copropagating, the phase matching condition can be written as,

$$\Delta k = 2k_P - n_{pr}k_{pr} \cos \theta - k_c \cos(-\theta). \quad (3.10)$$

which is shown in Fig. 3.3. This implies that the twin beams generated by the FWM process will have equal but opposite angles, which will be symmetric with respect to pump^[24]. This phase matching condition also governs the spatial distribution of the twin beams and leads to position-dependent quantum correlated subregions. The smallest correlated subregions of the twin beams is called the coherence area. Assuming that the FWM process occurs at a plane at the center of Rb cell, the plane that is an image of this cell center is called near field. Since the twin beams are generated on top of each other, in the near field the corresponding subregions of probe and conjugate will be correlated as shown in Fig. 3.4.

Typically the FWM process generates a single pair of entangled probe and conjugate beams. Taking advantage

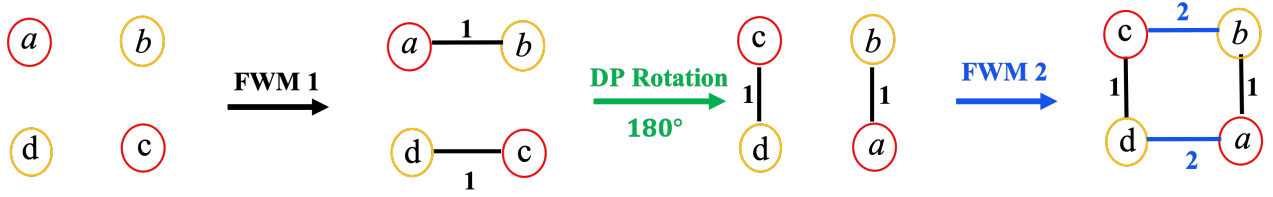


Figure 3.6: Modes a and c of the probe (red) get entangled with b and d of the conjugate (yellow) after FWM1 respectively. Modes a and c are then switched through a 180° rotation using a dove prism (DP). A second FWM, then entangles new combinations of modes, c - b and d - a , while preserving the entanglement between pairs a - b and c - d .

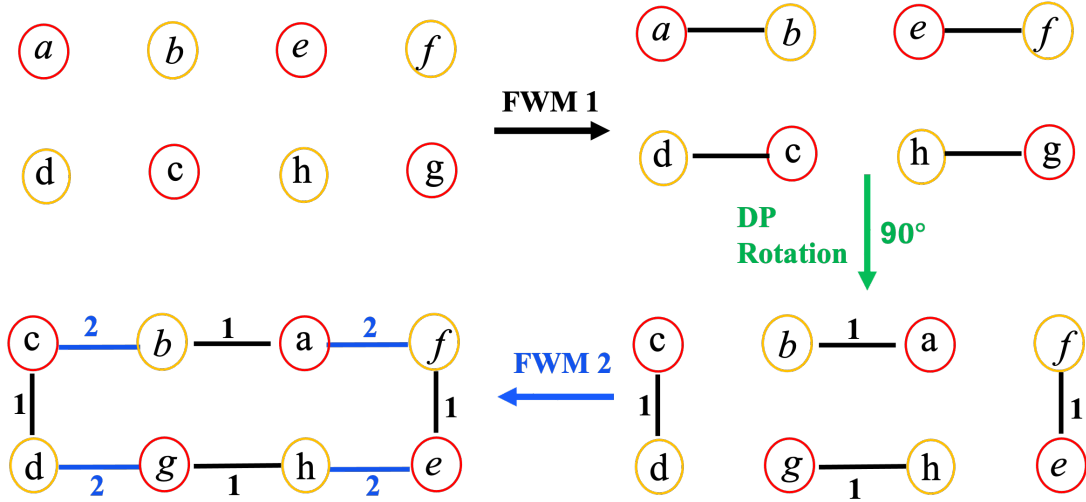


Figure 3.7: Four pairs of probe and conjugate modes get entangled through the first FWM process, i) a - b ii) e - f iii) g - h and iv) c - d . After displacing each probe mode to the location of next mode by a 90° rotation using DP, four new pairs get entangled through the second FWM process, thereby forming a connected graph.

of the multi-spatial mode nature of the twin beams, higher number of entangled probe-conjugate pairs can be generated through a single FWM process. This is achieved by making the spatial subregions independent of one other, which results in independently correlated pairs of subregions in the probe and conjugate after the FWM process. For this purpose, we are encoding spatial patterns with independent spatial regions in the probe beam that is used as the seed for the FWM process.

3.4 Generation of scalable multipartite entanglement

As described in Section 3.2, the twin beams generated through the FWM process are bipartite entangled. From previous discussions we saw that it is possible to generate multiple bipartite entangled pairs from a single FWM. It is possible to connect these bipartite entangled pairs to form quadrupartite or higher order entanglement via

a combination of rotation and a second FWM process^[13]. For example, consider the simplest case of the probe being encoded with a pattern consisting of two independent spatial regions as shown in Fig. 3.5. For ease of tracking, let's call the left circle a , right circle b and the corresponding conjugates as c and d , respectively, as shown in Fig. 3.6. The correlations introduced by FWM1 are shown by solid black lines. After FWM1 modes a and c are switched whereas the ordering of conjugate modes is unaltered. The switching is achieved by rotation using a Dove Prism (DP). Switched probe and unrotated conjugate are used to seed a second FWM process. The pairs of twin beams otherwise not entangled are entangled through the second process, thereby forming a connected graph.

This can be scaled up to higher number of modes by increasing the number of independent spatial regions encoded in the probe beam. Fig. 3.7 depicts the scenario of a four circle seed pattern. In this case, each probe mode is moved clockwise to the position of the next mode.

Chapter 4

Experimental Implementation and Results

In this chapter we discuss the experimental details and show preliminary results of intensity-intensity correlations between the pairs connected through the first (black) and second (blue) FWM processes and the lack of correlations for other pairs as expected. We also show that without any rotation from the DP, the pairs connected through the second process do not show any correlations, thereby verifying that the second set of connections is obtained by switching the modes. The beams required for the FWM process are generated from a CW Ti: Sapphire laser. A portion of the beam is separated using a beam sampler and passed through an acoustic optical modulator space (AOM) tuned to generate the probe beam at the desired frequency. The probe beam (red) and the intense pump beam (purple) are then passed through single mode optical fibers to obtain a clean spatial mode before the FWM process.

The setup consists of two FWM process with a DP in between for switching the modes as shown in Fig. 4.1. The probe coming out of the fiber is projected onto a Digital Light Processor (DLP) with a size of 3 mm in diameter to encode multiple spatial regions on a single beam. The DLP is a digitally controlled micromirror device that is also a spatial light modulator (SLM). The DLP can be programmed and controlled using its computer interface to encode an arbitrary pattern in the probe. The size of the probe is kept large at the plane of DLP so that all the active area of the DLP is illuminated by the incident probe. The beam reflected from the DLP is imaged to the first cell center using a $4f$ imaging system consisting of lenses $L_1=500$ mm and $L_2=500$ mm as shown in Fig. 4.1.

The orthogonally polarized intense pump beam with a beam size of 1.2 mm in diameter, and the weak probe beam reflected from the DLP intersect at an angle $\theta^{[24]}$ inside the center of the cell. The cell is 12 mm long, and its temperature is kept high to increase the atomic density to provide enough atoms to participate in the process. As a result of FWM, the probe beam (red) will experience gain and simultaneously the conjugate (yellow) is generated.

After FWM1, the pump, probe and conjugate are further imaged to the center of a second cell using another $4f$ system consisting of $L_3=500$ mm and $L_4=500$ mm. Using a dove prism, the position of the probe modes (red circles) is switched between the cells as shown in the Fig. 4.1. Since the rotation is done in a symmetric way, the degree of rotation is given by $\frac{360}{n}$, where n is the number of modes in each beam. A piezo is used to control

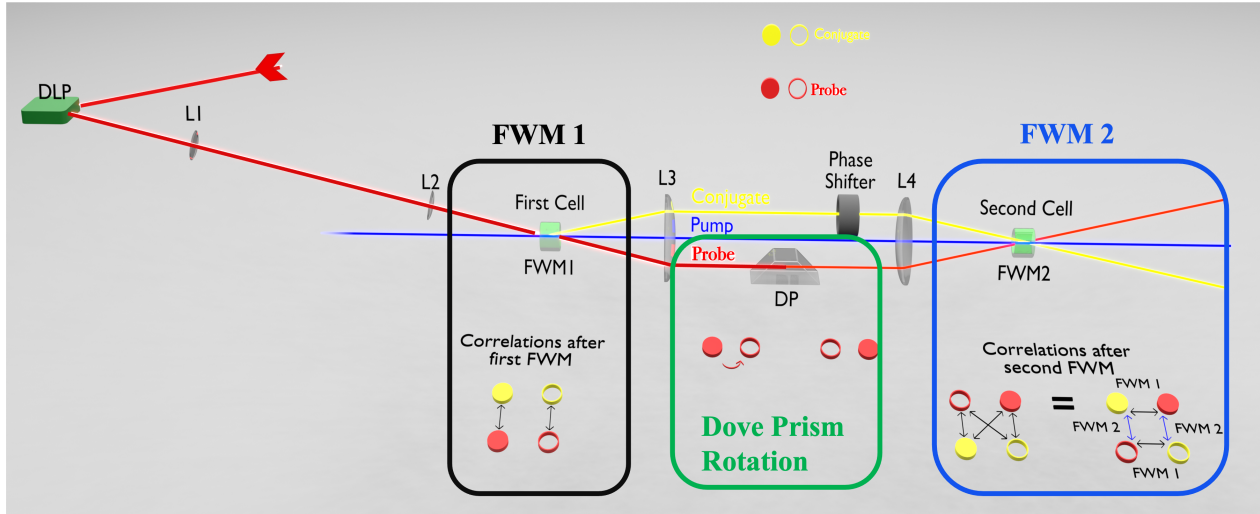


Figure 4.1: Modified SU(1,1) setup. The probe reflected from the DLP is imaged to the first cell center. The amplified probe (red), generated conjugate (yellow), and pump (blue) are imaged from the center of the first cell to the center of the second cell using another $4f$ imaging system. The spatial locations of circles in the probe are switched by rotating the beam by 180° using a dove prism in between the two processes.

the relative phase between the probe and conjugate. The system is locked at the maximum output power so that all measurements are taken at the same phase. For the two stage FWM process, the one photon detuning is scanned while the two photon detuning of the process is kept fixed. The optimum level of squeezing is obtained for a pump power of 150 mW, two photon detuning of $\delta = 5$ MHz and cell temperatures, $T_1 = T_2 = 112^\circ$.

4.1 Measurements of intensity-intensity correlations

The spatially separated modes enables us to select each pair of entangled modes individually and to measure quantum correlations. This is done by clipping the beam to select individual modes and then sending them into a detector connected to a spectrum analyzer to measure Intensity Difference Squeezing (IDS). For clipping, we need a clear cut image of both beams, which is achieved in the imaging plane. Hence, after the second FWM the beams are further imaged using another $4f$ imaging system consisting of two 500 mm lenses to yet another plane where they are clipped to select particular modes. The IDS results are shown in Figs. 4.2, 4.3 and 4.4. In Fig. 4.2, we can see the correlations between the different pairs of probe and conjugate modes. The SNL for a particular IDS trace is obtained by measuring the noise of a coherent state at the same power level. The IDS traces are then normalized with respect to their corresponding SNL. A squeezing of 4.2 dB is achieved without any clipping. The level of squeezing decreases for a single pair of modes, as expected when we are clipping, since we are breaking correlations between the selected and unselected pairs of modes thereby introducing additional noise. Multiple parameters such as pump power, temperature of the cell, intersecting angle, and detuning were optimized to obtain an efficient FWM. For the data plotted in Figs. 4.2, 4.3 and 4.4, all

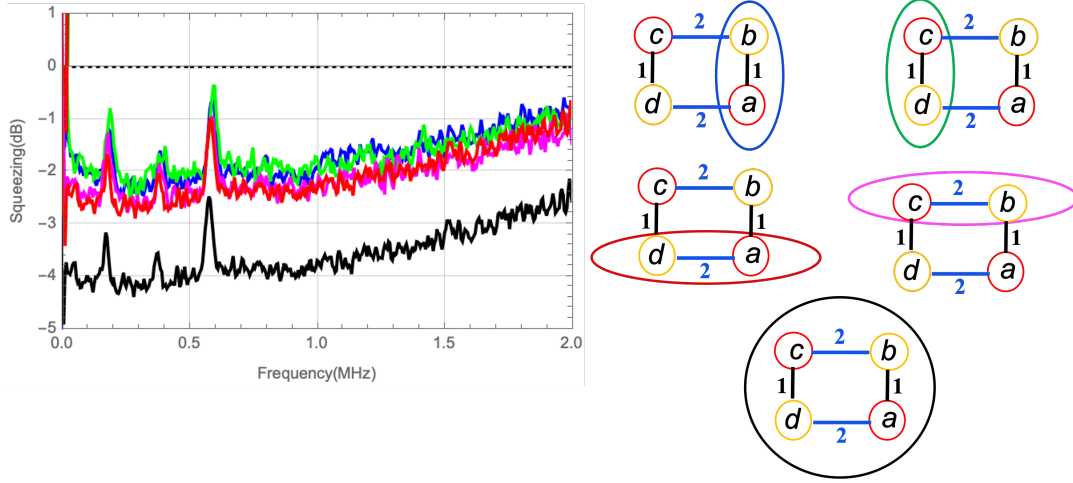


Figure 4.2: Correlation measurements of different pairs. The black trace corresponds to the IDS of the whole probe and conjugate after FWM2. The blue, green, red, and magenta traces correspond to IDS of the pairs shown on the right side with same color coding.

parameters affecting the FWM were kept constant to make the comparison accurate. The data was taken for a pump power of 150 mW and a cell temperature of 112°C for both cells which led to a gain of 2.5 for the second and 3 for the first FWM process. The contrast, also called the visibility determines the interference efficiency of the twin beams. The modified SU(1,1) had a contrast of 0.78 for the probe and 0.82 for conjugate.

4.2 Measurements of noise between uncorrelated modes

In contrast, if we measure the noise of uncorrelated pairs, that are not directly connected via either process, their individual noises add in quadrature. Figs. 4.3 and 4.4 show the noise spectra of the two modes in the probe and conjugate respectively, which are not correlated. As there are no correlations between the probe-probe and conjugate-conjugate modes, the noise of the individual modes added should match up with the noise measured directly from the uncorrelated pair. The peaks at the lower frequency is the noise introduced by the DLP, which is classical noise.

To verify that the correlations introduced by the second FWM (blue) are due to the rotation from the DP, we also measured the noise of different pairs without any DP rotation. As expected, when there is no switching of modes due to the DP, the pairs $a-d$ and $b-c$ are uncorrelated, as shown in Fig. 4.5.

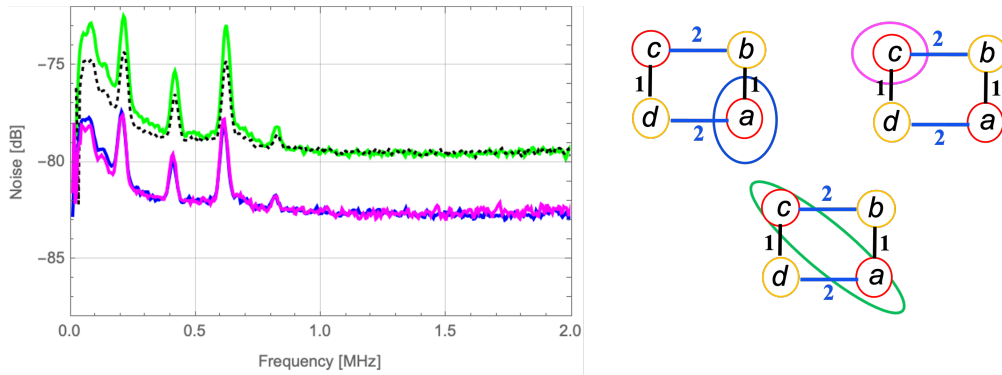


Figure 4.3: Noise traces for joint probe mode measurements. The two probe modes are not correlated with each other. The blue and magenta traces show the noise of the two probe modes. The dotted black trace is the noise of the uncorrelated pair measured using the detector. The green trace is given by blue and magenta traces added in quadrature, verifying that the noises of uncorrelated pair adds in quadrature .

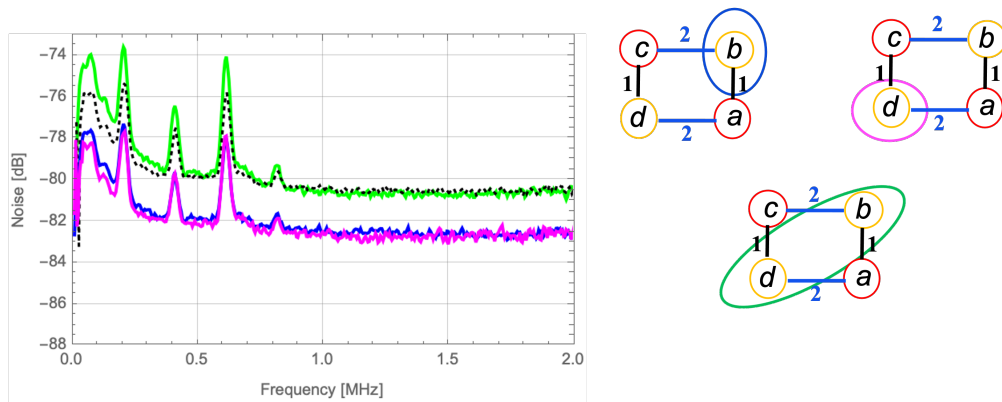


Figure 4.4: Noise traces for joint conjugate mode measurements. The two conjugate modes are not correlated with each other. The blue and magenta traces shows the noise of the two conjugate modes. The dotted black trace is the noise of the uncorrelated pair measured using the detector. The green trace is given by blue and magenta traces added in quadrature, verifying that the noises of uncorrelated pair adds in quadrature.

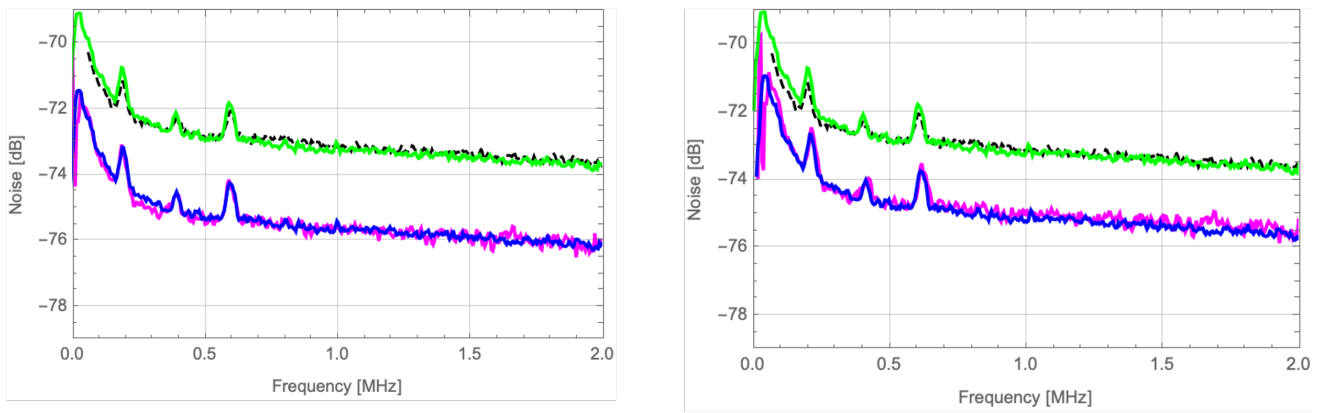


Figure 4.5: Correlation measurements without probe mode switching. The modes otherwise connected through the second FWM are uncorrelated without any DP rotation. The two figures shows the absence of correlation between the modes c - b and a - d without switching spatial locations. The dotted black line is the noise of the uncorrelated pair measured using the detector. The green trace is given by the blue and magenta traces added in quadrature, verifying that the noises of uncorrelated pair adds up in quadrature.

Chapter 5

Conclusion and future work

Through our experiment, we produced multi spatial mode correlations using a two stage FWM process. A squeezing of 4.2 dB is achieved and correlations are measured for expected entangled mode pairs. The results demonstrated in this report are for two modes in the probe and two in the conjugate. We also have the corresponding results for correlations for four modes in each beam, which shows the scalability of this technique. The DLP used for the spatial modulation works for any arbitrary pattern and hence this method can be used for scaling further to higher number of modes. However, the scaling is limited by the active area of DLP available to encode patterns. This technique for the generation of multiple modes within a single beam helps to reduce the losses introduced via cascaded FWM processes to a more compact and scalable platform. Even though squeezing can be evaluated using intensity-intensity difference measurements, we need another approach to verify entanglement. To prove ME, different combinations of quadratures must be measured simultaneously through a method called homodyne detection. For implementation of this detection technique we need a local oscillator (LO) that can be used as a reference beam. The LO should have the same mode, phase, and frequency as the probe and conjugate. Hence, we will require multiple local oscillators for homodyne detection. After the measurement of quadratures, the inequality violations discussed in Chapter 3 can be examined for the verification of entanglement. Even though the detection process is tedious, the generation process is scalable and the multi spatial mode correlations are a promising resource for multi channel quantum communications^[6].

Bibliography

- [1] C. M. Caves, “Quantum-mechanical noise in an interferometer,” *Physical Review D*, 1981.
- [2] A. Kumar, H. Nunley, and A. Marino, “Observation of spatial quantum correlations in the macroscopic regime,” *Physical Review A*, vol. 95, no. 5, p. 053849, 2017.
- [3] G. Nirala, S. T. Pradyumna, A. Kumar, and A. M. Marino, “Engineering spatial correlations in entangled twin beams,” Optical Society of America, 2021.
- [4] M. Dowran, A. Kumar, B. J. Lawrie, R. C. Pooser, and A. M. Marino, “Quantum-enhanced plasmonic sensing,” *Optica*, vol. 5, no. 5, pp. 628–633, 2018.
- [5] P. Grangier, R. Slusher, B. Yurke, and A. LaPorta, “Squeezed-light–enhanced polarization interferometer,” *Physical Review Letters*, vol. 59, no. 19, p. 2153, 1987.
- [6] S. L. Braunstein and P. Van Loock, “Quantum information with continuous variables,” *Reviews of Modern Physics*, vol. 77, no. 2, p. 513, 2005.
- [7] P. van Loock and S. L. Braunstein, “Multipartite entanglement for continuous variables: a quantum teleportation network,” *Physical Review Letters*, vol. 84, no. 15, p. 3482, 2000.
- [8] G. Jaeger, *Entanglement, information, and the interpretation of quantum mechanics*. Springer Science & Business Media, 2009.
- [9] K. N. Cassemiro and A. S. Villar, “Scalable continuous-variable entanglement of light beams produced by optical parametric oscillators,” *Physical Review A*, vol. 77, no. 2, p. 022311, 2008.
- [10] O. Pinel, P. Jian, R. M. De Araujo, J. Feng, B. Chalopin, C. Fabre, and N. Treps, “Generation and characterization of multimode quantum frequency combs,” *Physical Review Letters*, vol. 108, no. 8, p. 083601, 2012.
- [11] S. Armstrong, J.-F. Morizur, J. Janousek, B. Hage, N. Treps, P. K. Lam, and H.-A. Bachor, “Programmable multimode quantum networks,” *Nature Communications*, vol. 3, no. 1, pp. 1–8, 2012.

- [12] J.-i. Yoshikawa, S. Yokoyama, T. Kaji, C. Sornphiphatphong, Y. Shiozawa, K. Makino, and A. Furusawa, “Invited article: Generation of one-million-mode continuous-variable cluster state by unlimited time-domain multiplexing,” *APL Photonics*, vol. 1, no. 6, p. 060801, 2016.
- [13] S. Kim and A. M. Marino, “Scalable genuine multipartite entanglement with parametric amplifier networks,” in *Frontiers in Optics*, pp. FW7C–4, Optical Society of America, 2020.
- [14] D. F. Walls and G. J. Milburn, *Quantum optics*. Springer Science & Business Media, 2007.
- [15] R. Loudon and P. L. Knight, “Squeezed light,” *Journal of Modern Optics*, vol. 34, no. 6-7, pp. 709–759, 1987.
- [16] M. Dowran, “Quantum plasmonic sensing using squeezed light,” 2021.
- [17] G. S. Agarwal, *Quantum optics*. Cambridge University Press, 2012.
- [18] R. Teh and M. Reid, “Criteria for genuine N -partite continuous-variable entanglement and Einstein-Podolsky-Rosen steering,” *Physical Review A*, vol. 90, no. 6, p. 062337, 2014.
- [19] B. P. A. Einstein and N. Rosen, “Can quantum-mechanical description of physical reality be considered complete?,” *Physical Review*, vol. 47, no. 2, p. 777, 1935.
- [20] L.-M. Duan, G. Giedke, J. I. Cirac, and P. Zoller, “Inseparability criterion for continuous variable systems,” *Phys. Review Letters*, vol. 84, pp. 2722–2725, Mar 2000.
- [21] S. L. Braunstein and D. D. Crouch, “Fundamental limits to observations of squeezing via balanced homodyne detection,” *Physical Review A*, vol. 43, no. 1, p. 330, 1991.
- [22] P. Van Loock and A. Furusawa, “Detecting genuine multipartite continuous-variable entanglement,” *Physical Review A*, vol. 67, no. 5, p. 052315, 2003.
- [23] R. Boyd, *Nonlinear optics*. Academic Press, 1992.
- [24] M. Turnbull, P. Petrov, C. Embrey, A. Marino, and V. Boyer, “Role of the phase-matching condition in nondegenerate four-wave mixing in hot vapors for the generation of squeezed states of light,” *Physical Review A*, vol. 88, no. 3, p. 033845, 2013.